

2 | Computational Methodology

In this chapter, the theories and the models used for electronic structure calculations along with optical properties are briefly introduced to provide a foundational understanding of the photocatalytic systems studied in this thesis. This chapter covers the history and evolution of the first-principles technique based on DFT, which serves as the main investigative instrument in this thesis. We start with the basic formulations of the Kohn-Sham method, which forms the basis of DFT and is used in our calculations utilizing Quantum Espresso and WIEN2k codes.

Learning about the energetics and the bonding inside photocatalysts/molecules or between molecules and a photocatalytic surface is necessary to investigate the surface properties and chemical processes. One can examine the system of interest and gain this knowledge through electronic structure computation. The electronic structure problem is roughly solved to get the energetics of model catalytic systems at a desired precision level with an acceptable computational cost by advancements in theoretical approaches.

The efficient way to describe simple quantum systems like the hydrogen atom [47] is through the development of quantum theory and theoretical tools like the time-independent Schrödinger equation [47] (given in Eq. 2.1, where the single-particle eigen function is $\psi(\vec{r})$, the associated eigenvalue is E , and the system Hamiltonian is \hat{H}). The hydrogen atom system is the simplest toy model—a two-body system with a single proton and electron—in which the ground state energy of -13.6 eV may be obtained by numerical computation of the Schrödinger equation using a variable separable approach. The process of solving the Schrödinger equation becomes more difficult as a system gets larger, for example in the case of the helium atom. This is because there are more variables involved in such many body systems, which makes it difficult to find the exact numerical solution. This difficulty can be overcome by splitting the system into a two-body system with a reduced mass.

$$-\frac{\hbar^2}{2m}\hat{H}\psi(\vec{r}) = E\psi(\vec{r}) \quad (2.1)$$

$$\hat{H} = \hat{T}_e + \hat{T}_n + \hat{V}_{e,e} + \hat{V}_{e,n} + \hat{V}_{n,n} \quad (2.2)$$

But when we take into account the periodic arrangement of atoms in solids which are thought of as many-electron systems with indistinguishable mutual interactions in a smeared-out background positive nuclear charge, the complexity increases exponentially. The 'N' particle eigen function $\psi(\vec{r}_1, \vec{r}_2, \vec{r}_3, \dots, \vec{r}_N)$ [48] describes such a system. Finding the precise solution to a many-body system with this complication is nearly impossible. Furthermore, we also encounter complex interactions between electrons-nuclei as well as between electrons-electrons, which contribute to the complexity of the system's Hamiltonian, as seen in Eq. 2.2. The kinetic and

potential energy operators for electron-electron, electron-nuclei, and nuclei-nuclei (where e is denoted for electron and n for nuclei) interactions are denoted by the following expressions: \hat{T}_e , \hat{T}_n , $\hat{V}_{e,e}$, $\hat{V}_{e,n}$, and $\hat{V}_{n,n}$.

Subsequently, the Schrödinger equation, in its many-body time-independent version, reduces to Eq. 2.3, in which the electrons and nuclei are represented by the indices i and k ; the masses of the electrons and nuclei are m_e and m_n ; the nuclear charges on the nuclei are Z_k and $Z_{k'}$; the radial distances between nuclei-nuclei, electron-electron, and electron-nuclei, are represented by the values of $|r_{n,k}^{\vec{r}} - r_{n,k'}^{\vec{r}}|$, $|\vec{r}_i - \vec{r}_j|$, and $|\vec{r}_i - r_{n,k}^{\vec{r}}|$, respectively. When Eq. 2.3 is solved, information about the system's ground state in terms of energy eigenvalues is obtained. Since this equation depends on the atomic mass and charge of the electrons and nuclei, solving it without the need for parametric fitting as in the case with empirical problems, this method is referred to as the first principles.

$$\begin{aligned} \hat{H} = & -\frac{\hbar^2}{2m_e} \sum_i \frac{\partial^2}{\partial r_i^2} - \frac{\hbar^2}{2m_n} \sum_k \frac{\partial^2}{\partial r_{n,k}^2} + \frac{1}{2} \sum_{\substack{k,k' \\ k \neq k'}} \frac{e^2}{4\pi\epsilon_0} \frac{Z_k Z_{k'}}{|r_{n,k}^{\vec{r}} - r_{n,k'}^{\vec{r}}|} \\ & + \frac{1}{2} \sum_{\substack{i,j \\ i \neq j}} \frac{e^2}{4\pi\epsilon_0} \frac{1}{|\vec{r}_i - \vec{r}_j|} + \sum_i \sum_j \frac{e^2}{4\pi\epsilon_0} \frac{Z_k}{|\vec{r}_i - r_{n,k}^{\vec{r}}|} \end{aligned} \quad (2.3)$$

Nevertheless, the related complexities continue to exist, rendering the solution of Eq. 2.3 for the many-body system unattainable. Born and Oppenheimer attempted to solve this problem and got the equation into solvable form.

2.1 Wave function Based Approach

2.1.1 Born Oppenheimer Approximation

Take a look at the cartoon example in Fig. 2.1 to see why DFT [49] and the Kohn-Sham equations represent such a significant advancement in physics and chemistry. In the figure, there is an elephant and some bees, representing a nucleus and electrons. The complex motion of bees around the elephant represents the

interactions among the electrons. Our task is to mobilize the entire group to reach the maximum degree of stability. This is undoubtedly a challenging issue, and it becomes worse as there are too many "bodies." We might simplify it by using the Born-Oppenheimer approximation [50], which states that we do not have to concurrently optimize every particle's position if the "elephant" moves slowly and sluggishly in comparison to the flying "bees". The elephant can be kept motionless, and we just need to optimize the bees' locations for each fixed position of the elephant. This is still a challenging many-body problem to solve, though, because there are a lot of bees and they are interacting with one another. In the same way, the electrons would pass with greater momentum than the nuclei when they are both contained in a momentum space under mass. Thus, the Born-Oppenheimer approximation allows us to ignore the nuclei contribution in the Hamiltonian given in Eq. 2.2. In light of this, it is hypothesized that the electrons move in a positive background potential that is scattered out and originates from the comparatively static nucleus. Then, the eigenfunction of electrons and nuclei may be combined to provide the total eigenfunction. Consideration of the Born-Oppenheimer approximation results in the reduced form of Schrödinger equation removing the nuclear kinetic and potential energy operator and addition of an external potential operator shown in Eq. 2.31.

$$-\frac{\hbar^2}{2m} \hat{H} \phi(\vec{r}) = \left(-\frac{\hbar^2}{2m_e} \sum_i \frac{\partial^2}{\partial \vec{r}_i^2} + \frac{1}{2} \sum_{\substack{i,j \\ i \neq j}} \frac{e^2}{4\pi\epsilon_0 |\vec{r}_i - \vec{r}_j|} + \hat{V}_{e,n} + \hat{V}_{ext} \right) \phi(\vec{r}) = E \phi(\vec{r}) \quad (2.4)$$

Since this approximation ignores the antisymmetric nature of Fermionic wavefunction and complex electron-electron interactions like correlations it only partially resolves the complexity of the many-body Schrödinger equation. The Hartree and Hartree-Fock approximations addressed this.

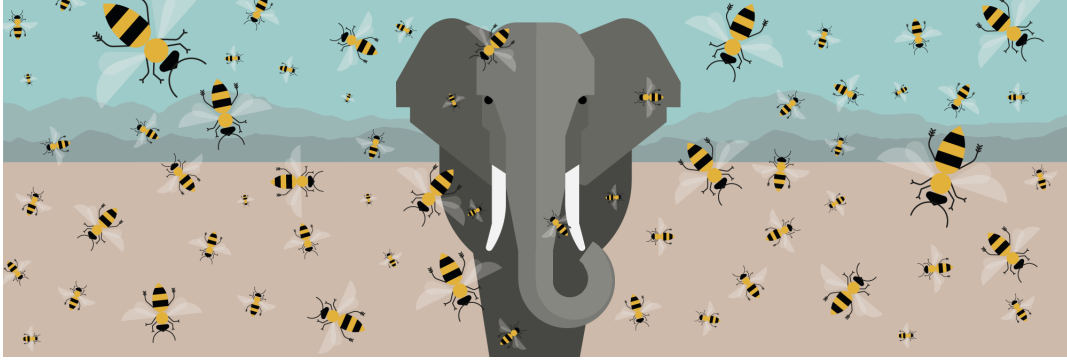


FIGURE 2.1: Picture of an elephant surrounded by numerous bees representing the sluggish-nuclei, and electrons orbiting, respectively around it .

2.1.2 Hartree and Hartree-Fock Method

To further simplify the many-body issue, the coulomb interactions between electrons regulated by classical electrostatics have to be addressed. This was accomplished by Hartree [51], who transformed the many-body issue into the independent electron approximation, or one-electron problem. The Born-Oppenheimer-modified Hamiltonian is influenced by the electron-electron interaction potential, which is independent of self-interactions. The distribution of electronic charge density in space $[n(\vec{r})]$ results in an electrostatic potential $V_l(\vec{r})$, which is controlled by Poisson's (Eq. 2.5) relation, according to classical electrostatics. Then, the individual eigenstates can be summed over the occupied eigenstates to construct the charge distribution $(\rho(\vec{r}), \text{Eq. 2.6})$ corresponding to the Hartree potential. The Hartree potential $(V_H(r))$ would be the potential energy of the electrons in such an electrostatic potential.

$$\nabla^2 V_l(\vec{r}) = \frac{\rho(\vec{r})}{\epsilon_0} \quad (2.5)$$

$$\rho(\vec{r}) = \sum_m |\psi_m(\vec{r})|^2 \quad (2.6)$$

This results in the potential for electron-electron interaction being reduced to that of a single electron. In addition, Hartree proposed that the many-body eigenfunction be represented as the product of the eigenfunctions of each electron in the system. This means that the Hartree equation shown in Eq. 2.7, which is derived by adding the Hartree potential, is a modified version of the Schrödinger equation.

The electron correlations that Hartree neglected to mention, however, were the missing component that resulted in the Hartree-Fock approximations [52].

$$\left(\frac{\hbar^2}{2m_e} \sum_i \frac{\partial^2}{\partial \vec{r}_i^2} + \sum_{m \neq l} \int \frac{|\psi_m(r)|^2}{|r - r'|} dr' + \hat{V}_{e,n} + \hat{V}_{ext}\right) \psi(\vec{r}) = E \psi(\vec{r}) \quad (2.7)$$

The two main issues with the Hartree approach were that (i) the electron-electron interactions were averaged and (ii) the electron eigen functions were not anti-symmetric for the electron exchange.

Hartree-Fock's approach solves the issue raised by Slater and Fock, independently [53, 54]. They started with an anti-symmetric eigenfunction as a function of spin and position, which complies with the Pauli exclusion rules, which demands that the eigenfunctions be anti-symmetric under particle exchange. Consequently, electrons with the same spin cannot concurrently occupy the same eigenstate, meaning that no two electrons can have the same set of quantum numbers. Additionally, they employed the Slater determinant eigenfunction, which is a one-electron eigenfunction ($\psi_i(\vec{r}_j, \sigma_j)$) that fulfills anti-symmetry and is given in Eq. 2.8, rather than the sum of eigenfunctions.

$$S = \frac{1}{\sqrt{N!}} \begin{vmatrix} \psi_1(\vec{r}_1, \sigma_1) & \psi_1(\vec{r}_2, \sigma_2) & \cdots & \psi_1(\vec{r}_N, \sigma_N) \\ \psi_2(\vec{r}_1, \sigma_1) & \psi_2(\vec{r}_2, \sigma_2) & \cdots & \psi_2(\vec{r}_N, \sigma_N) \\ \vdots & \vdots & \cdots & \vdots \\ \psi_N(\vec{r}_1, \sigma_1) & \psi_N(\vec{r}_2, \sigma_2) & \cdots & \psi_N(\vec{r}_N, \sigma_N) \end{vmatrix} \quad (2.8)$$

$$\begin{aligned} & \left(\frac{\hbar^2}{2m_e} \sum_i \frac{\partial^2}{\partial \vec{r}_i^2} + \sum_{m \neq l} \int \frac{|\psi_m(r)|^2}{|r - r'|} dr' \right) \\ & + \hat{V}_{e,n} + \hat{V}_{ext} - \sum_m \delta_{S_m, S_l} \int \frac{\psi_m^*(r') \psi_l(r')}{|r - r'|} dr' \psi(\vec{r}) = E \psi(\vec{r}) \end{aligned} \quad (2.9)$$

Next, by minimizing the Hamiltonian's expectation value using the Lagrangian multiplier approach, we arrived at the set of Hartree-Fock equations shown in Eq. 2.9, where the spin labels are s_m and s_l . This resolves the issue of the electron

exchange but the approach requires high computational facilities, as the total energy minimization is to be performed for the 'N' particle Slater determinant. The many-body Schrödinger equation is complicated because it has $3N$ degrees of freedom for a system with 'N' electrons, increasing the number of variables in the problem. This problem is solved by DFT, which approximates the many-body problem to a single, computationally feasible electronic density.

2.2 Development of Density Functional Theory

Density functional theory (DFT) [55, 56] is widely used in physics and chemistry to calculate the properties of many-electron systems. The electron density ($[n(\vec{r})]$) of ground states is related to every property of a many-body system. By considering the electron density, DFT enables us to get around the computational challenge of calculating the many-body wave function. The challenge of calculating the ground state energy and particle density of an N-electron system has been reformulated by Kohn and Sham [55] as the task of solving a system of independent-particle equations. These Kohn–Sham equations are substantially simpler to solve than the original ($3N$ -dimensional) many-body problem. They are composed of N single-particle (three-dimensional) Schrödinger-like equations with a modified effective potential. The modified potential incorporates a contribution from the quantum-mechanical exchange and correlation of the particles and is a function of the total particle density.

2.2.1 Thomas-Fermi Method

Thomas and Fermi suggested that instead of taking into account the single particle eigenfunctions suggested by Hartree and Hartree-Fock methods, the overall energy of a system may be expressed as a functional of the electron density. Consequently, the electron density may be used to describe the kinetic energy of a set of 'N' interacting electrons. Subsequently, the overall energy (E) can be represented as an

electron density functional. Then, Thomas-Fermi's formulation may be reduced by using the Lagrangian multiplier approach. Nevertheless, this method's drawback is that it ignores electron exchange. Dirac addressed the issue by incorporating the correlation functional and exchange interaction, but it was still impossible to determine the shell structure and atomic behavior for the complicated systems.

2.2.2 Hohenberg-Kohn-Sham Approach

Hohenberg-Kohn theorems:

Theorem 1 (Existence theorem) - The ground state particle density $[n_0(\vec{r})]$ determines the potential $V_{ext}(\vec{r})$ for any system of interacting particles in an external potential $V_{ext}(\vec{r})$, except a constant [56].

Theorem 2 (Variational principle) - For any given external potential $V_{ext}(\vec{r})$, a universal functional for the energy $E[n]$ may be constructed in terms of the density $[n(\vec{r})]$. The global minimum value of this functional, for any given $V_{ext}(\vec{r})$, is the exact ground state of the system; the exact ground state density $[n_0(\vec{r})]$ is the density that minimizes the functional.

It was demonstrated by Hohenberg and Kohn that the total energy of an electron gas, including correlation and exchange, is a unique functional of the electron density, even in the presence of a static external potential. The system's ground-state energy, expressed as the minimal value of the total energy functional, is produced by the precise single-particle ground-state density, which is represented by this density.

Kohn-Sham ansatz:

The density of an additional non-interactive independent particle system is equal to the ground state density of the many-body interacting system. The ground state energy functional expression for an interacting system is expressed as follows using the Kohn-Sham method [55]:

$$E_{Kohn-Sham}[n(\vec{r})] = T[n(\vec{r})] + E_{ext}[n(\vec{r})] + E_{Hartree}[n(\vec{r})] + E_{xc}[n(\vec{r})] \quad (2.10)$$

The electron-electron interaction, denoted by $E_{Hartree}$ under the Hartree approximation, the external potential denoted by E_{ext} , and the kinetic energy of the non-interacting electrons in $\phi_i(\vec{r})$ are provided as follows:

$$E_{Hartree}[n(\vec{r})] = \iint \frac{n(\vec{r})n(\vec{r}')}{|\vec{r} - \vec{r}'|} d\vec{r} d\vec{r}' \quad (2.11)$$

$$E_{ext}[n(\vec{r})] = \int \hat{V}_{ext} n(\vec{r}) d\vec{r} \quad (2.12)$$

$$T[n(\vec{r})] = \sum_i \int \phi_i^*(\vec{r}) \left(-\frac{1}{2} \nabla^2\right) \phi_i(\vec{r}) d^3 r' \quad (2.13)$$

The remaining quantity $E_{xc}[n(\vec{r})]$, is the exchange-correlation energy found in Eq. 2.10. The Kohn-Sham equation, which is represented in Eq. 2.14 below, is an effective single electron equation that results from the variation of the total energy functional concerning the single electron orbitals $\phi_i(\vec{r})$, which are variational values.

$$-\frac{1}{2} \nabla^2 \phi_i(\vec{r}) + \hat{V}_{ext}[(n(\vec{r}))] \phi_i(\vec{r}) + \int \frac{n(\vec{r}')}{|\vec{r} - \vec{r}'|} d\vec{r}' \phi_i(\vec{r}) + \frac{\delta E_{xc}(n(\vec{r}))}{\delta(n(\vec{r}))} \phi_i(\vec{r}) = \epsilon_i \phi_i(\vec{r}), \quad (2.14)$$

$$V_{eff}(\vec{r}) = V_{ext}[(n(\vec{r}))] + \int \frac{n(\vec{r}')}{|\vec{r} - \vec{r}'|} d^3 r' + \frac{\delta E_{xc}(n(\vec{r}))}{\delta(n(\vec{r}))} \quad (2.15)$$

Eq. 2.15 provides the Kohn-Sham equation for electrons in a potential, where the exchange-correlation potential is determined by varying the exchange-correlation energy. As a result, the Kohn-Sham equation may be expressed in the following modified form:

$$\left(-\frac{1}{2} \nabla^2 + V_{eff}(\vec{r})\right) \phi_i(\vec{r}) = \epsilon_i \phi_i(\vec{r}) \quad (2.16)$$

Self Consistent Field Cycle

The flow diagram in Fig. 2.2 illustrates the series of actions necessary to do a total energy pseudopotential calculation using standard matrix diagonalization techniques. To compute the exchange-correlation potential and the Hartree potential, the process first requires an estimate of the electronic charge density. To derive the Kohn-Sham eigenstates [55], the Hamiltonian matrices for each of the k

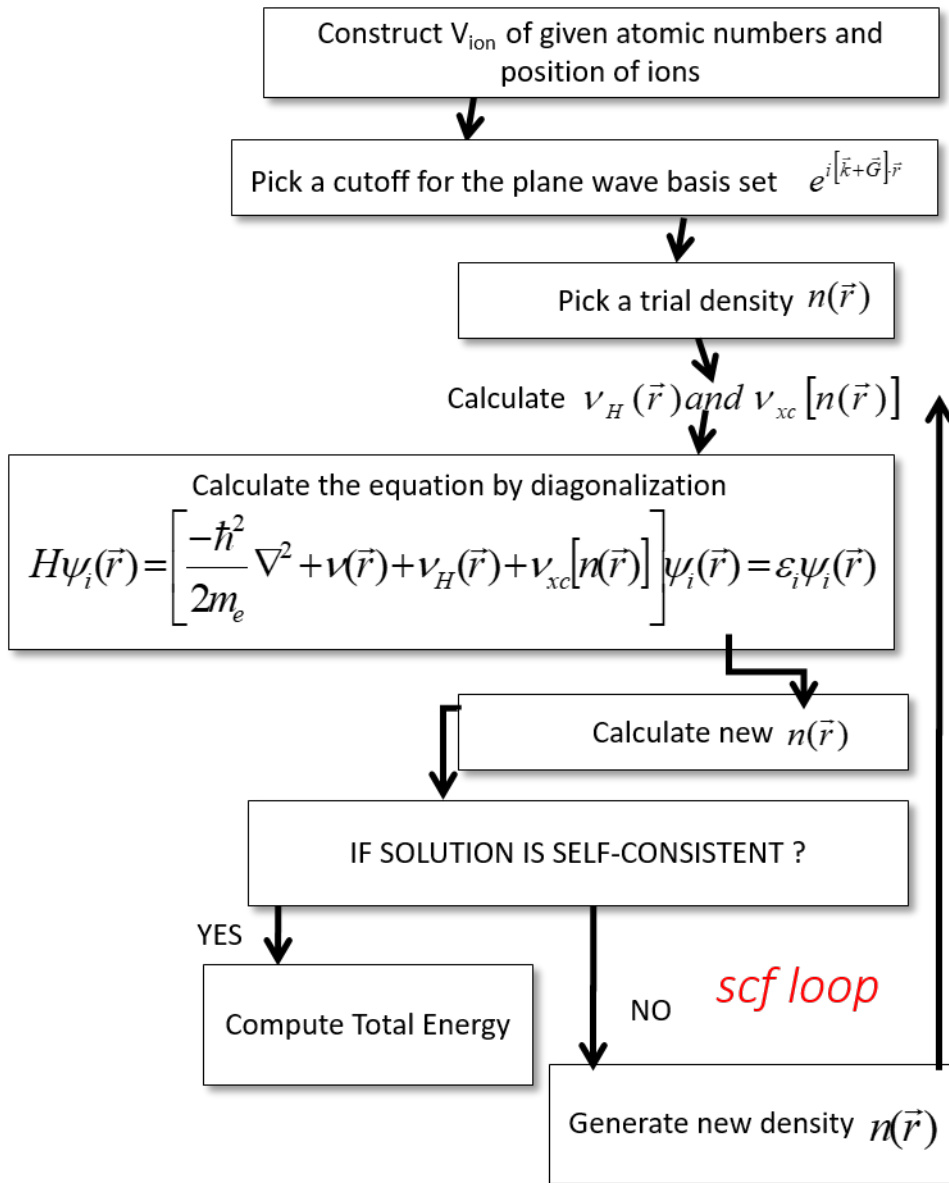


FIGURE 2.2: Flow diagram (Self-consistent field cycle) showing the steps involved in computing a solid's total energy using traditional matrix diagonalization.

points included in the computation must be built and diagonalized. A new set of Hamiltonian matrices must be built using the new electronic potentials as these eigenstates often provide a different charge density than the one that was initially utilized to build the electronic potentials.

The procedure is continued until the solutions are self-consistent after obtaining the eigenstates of the new Hamiltonians. Since this accelerates the convergence to self-consistency, the new electronic potential is thought to be a mixture of the

electronic potentials produced by the old and the new eigenstates. Tests should be run to make sure that the total energy converges as a function of the cutoff energy for the plane-wave basis set as well as the number of k points to finish the total energy calculation. A cutoff energy and k-points are selected in such a way that they lead to the convergence of energy within the given computational facilities, hence the convergence threshold is set which helps in energy convergence, and once this threshold energy difference is reached, further calculations are performed.

2.3 Exchange and Correlation Functional

The Kohn-Sham approach's exchange and correlation functionals specify the precision of computations and results. Many functionals have been produced since the theory's inception to accurately predict chemical properties. In general, they may be categorized and comprehended using Jacob's ladder of energy functionals, wherein the computational expense rises as one climbs the ladder toward a precise chemical depiction of the system being studied. The functionals for exchange and correlation must adhere to specific requirements. Specifically, they must: (i) have slowly varying densities and reduce to a homogenous two-dimensional electron gas limit; (ii) be asymptotic for atoms/molecules (represented as $V_{xc}[n(\vec{r})] \rightarrow -\frac{1}{\vec{r}}$) for $\vec{r} \rightarrow \infty$); and (iii) not exhibit self-interacting behavior. These functionals fall into one of the three categories: local, semi-local, and non-local.

2.3.1 Local and Semi-Local functionals

Since the exchange energy functional relies on the electron density and spin at a particular position \vec{r} in the electron cloud of an atom described by Eq. 2.17, local density approximations (LDA) [57] are referred to as local functionals. Conversely, the functionals known as semi-local functionals are the Generalized Gradient Approximations (GGA) Eq. 2.18, as the energy functional is dependent on the electron density and their gradients at the same place \vec{r} and its surroundings. Among

the most popular and extensively utilized semi-local functionals is PBE-GGA[58].

$$E_{xc}^{LDA}[n(\vec{r})] = \int \epsilon_{xc}[n(\vec{r})]n(\vec{r})d^3r \quad (2.17)$$

$$E_{xc}^{GGA}[n(\vec{r})] = \int \epsilon_{xc}[n(\vec{r}), \nabla n(\vec{r})]n(\vec{r})d^3r \quad (2.18)$$

2.3.2 Non-Local functionals

Hybrid functionals are a family of non-local functionals that are more desired than other approximations because they yield chemically precise results, despite their high computing cost. Within these functionals, the energy functional is contingent upon the density of orbitals present across the atom's electron cloud. These functionals have the following advantages: (i) we can eliminate the self-interaction terms; (ii) for high \vec{r} , we can obtain the right asymptotic form ($-\frac{1}{r}$). Since the LDA exchange and correlation errors cancel each other out and the LDA correlation errors are significantly larger than the exchange errors, the straightforward answer is to construct an exchange-correlation energy functional. In other words, the solution is obtained by modifying Eq. 2.19 by adding a mixing parameter (α ; $0 < \alpha < 1$) for the PBE0 functional, this results in Eq. 2.20 for the Quantum Espresso code, whilst Eq. 2.21 and Eq. 2.22 represents it for WEIN2k [59]. The coulomb operator in this functional (HSE06 [60, 61]) is divided into two parts: the short-ranged (SR) and the long-ranged (LR) parts. The short-range exchange fraction (α) for the SR part is set to 0.25. The screening parameter, ω , controls the extent of short-range interactions, and we have taken into consideration the variable value of ω depending on the supercell and the k-points considered for scf calculation for consistent energy gap values in semiconducting solids.

$$E_{xc}^{HSE} = \alpha E_x^{HF,SR}(\omega) + (1 - \alpha)E_x^{PBE,SR}(\omega) + E_x^{PBE,LR}(\omega) + E_C^{PBE}(\omega) \quad (2.19)$$

$$E_{xc}^{HSE} = \frac{1}{4}E_x^{HF,SR}(\omega) + \frac{3}{4}E_x^{PBE,SR}(\omega) + E_x^{PBE,LR}(\omega) + E_C^{PBE}(\omega) \quad (2.20)$$

$$E_{xc}^{hybrid} = E_{xc}^{SL} + \alpha_x (E_x^{(scr)HF} - E_x^{(scr)SL}) \quad (2.21)$$

$$E_x^{(scr)HF} = -\frac{1}{2} \sum_{i=1}^N \sum_{j=1}^N \delta_{\sigma_i \sigma_j} \iint \psi_i^*(\vec{r}) \psi_j(\vec{r}) \times v(|\vec{r} - \vec{r}'|) \psi_j^*(\vec{r}') \psi_i(\vec{r}') d^3r d^3r' \quad (2.22)$$

2.4 Electronic Approximation Methods

2.4.1 Plane Wave and Pseudopotential

Blöch's theorem (Eq. 2.23) [62] asserts that a discrete plane-wave basis set may be used to extend the electronic wave functions at each periodic k-point. Expanding the electronic wave functions, in theory, requires an indefinite plane-wave basis set. Consequently, it is possible to truncate the plane-wave basis set so that it only contains plane waves with kinetic energies below a certain cutoff energy. Regardless of the cutoff energy, the basis set would always be infinitely vast since each electronic wave function needs a continuum of plane-wave basis states to accurately describe the wavefunction [2, 63].

$$\Psi_k^n(\vec{r}) = \sum_{\vec{K}} c_{\vec{K}}^{n,\vec{k}} e^{i(\vec{k} + \vec{K})\vec{r}}, \quad (2.23)$$

However, a plane-wave basis set is typically not well suited for depicting electronic wave functions, because a very large number of plane waves are required to expand the tightly bound core orbitals and to follow the rapid oscillations of the valence electron wave functions in the core region. To execute an all-electron calculation, a very large plane-wave basis set would be needed, and calculating the electronic wave functions would take a very long time.

The electronic wave functions can be expanded with a significantly reduced number of plane-wave basis states according to the pseudopotential approximation

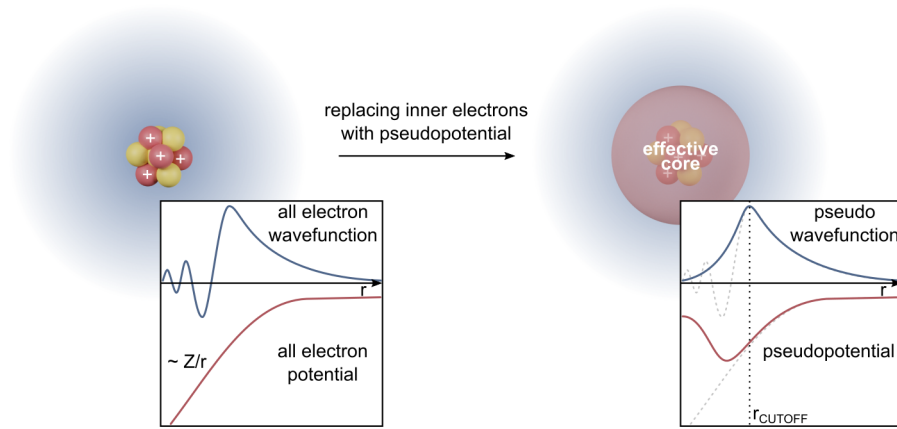


FIGURE 2.3: Schematic representation of the associated wave functions for the all-electron (solid lines) and pseudoelectron (dashed lines) potentials. The suggested radius (r_c) is the one at which the values of all electrons and pseudo-electrons match. [2].

where valence electrons influence most of a solid's physical characteristics than core electrons. The pseudopotential approximation works on a set of pseudo wave functions rather than valence wave functions by eliminating the core electrons and substituting them, with a weaker pseudopotential. The most general form for a pseudopotential is:

$$V_{NL} = \sum_{lm} |lm\rangle V_l \langle lm|, \quad (2.24)$$

Here, the pseudopotential for angular momentum l is V_l , and the spherical harmonics are $|lm\rangle$. The scattering from the pseudopotential must be angular momentum dependent because the phase shift caused by the ion core varies for each angular momentum component of the valence wave function. Fig. 2.3 shows a schematic illustration of an ionic potential, valence wave function, and the associated pseudopotential and pseudo wave function. Because of the significant ionic potential in the region inhabited by the core electrons, the valence wave functions fluctuate rapidly in this area. The ideal construction of the pseudopotential is to have no radial nodes in the core region of the pseudo-wave functions but to have scattering properties or phase shifts for the pseudo-wave functions that are identical to the scattering properties of the nuclei and the core electrons for the valence wave functions. Over time, various types of pseudopotentials have been produced, including ultra-soft, projector-augmented wave, norm-conserving, and others [64–66]. In

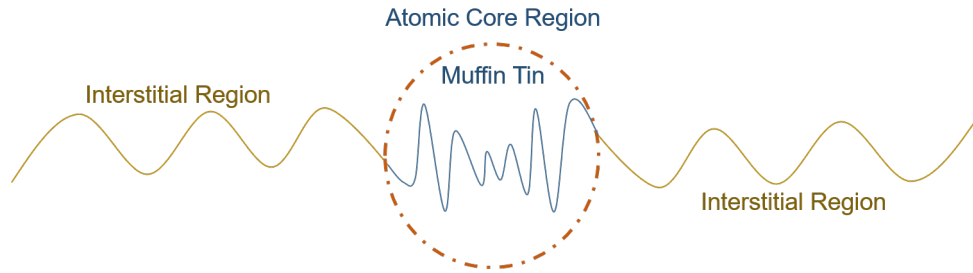


FIGURE 2.4: The FP-LAPW method's Muffin-Tin (MT) spherical area and Interstitial region.

this study, we have considered ultra-soft and norm-conserving pseudopotential including core correction for structural relaxation and scf calculations, respectively.

2.4.2 Full Potential Linearized Augmented Plane Wave Method

The linearized augmented plane wave (LAPW) approach [59, 67], like most methods for the representation of wave functions, involves introducing a basis set that is specifically tailored to the issue to solve the Kohn-Sham equations for the ground state density, total energy, and (Kohn-Sham) eigenvalues (energy bands) of a many-electron system (in this case, a crystal). For the consideration of exchange and correlation, it is based on DFT and makes use of the local spin density approximation (LSDA), among other things. The literature has a variety of LSDA potentials, but more contemporary versions that make use of the GGA are also accessible. Relativistic effects can be included in a scalar relativistic treatment of valence states or in a second variational technique that includes spin-orbit coupling. Complete relativistic treatment is given to core states. By splitting the unit cell into non-overlapping atomic spheres (centered at the atomic sites) and an interstitial area, this adaptability is accomplished. Different basis sets are employed in these two categories of areas, as follows: A linear combination of radial functions times spherical harmonics Y_{lm} is utilized inside the atomic sphere $t(S_t)$. As shown in Fig. 2.4, for the interstitial region a plane wave expansion is utilized.

LAPW has the following mathematical representation:

$$\Phi_{\mathbf{K}_n} = \begin{cases} \sum_{lm} [A_{lm,\mathbf{k}_n} u_l(r, E_l) + B_{lm,\mathbf{k}_n} \dot{u}_l(r, E_l)] Y_{lm}(\hat{r}), & r \in S_t \\ \frac{1}{\sqrt{\omega}} e^{i\mathbf{k}_n \cdot \vec{r}}, & r \in I, \end{cases} \quad (2.25)$$

where $u_l(r, E_l)$ is the energy derivative of u_l evaluated at the same energy E_l ; $u_l(r, E_l)$ is the regular solution of the radial Schrödinger equation for energy E_l (normally chosen at the center of the corresponding band with the l-like character) and the spherical part of the potential inside sphere t . The radial function is formed by a linear combination of these two functions; the coefficients A_{lm} and B_{lm} are functions of k_n that are obtained by demanding that this basis function coincide (in value and slope) with the corresponding basis function of the interstitial region for each plane wave (PW). Here, the reciprocal lattice vector is $k_n = k + K_n$; K_n , and the wave vector inside the first Brillouin zone is \mathbf{k} . In every atomic sphere, an atomic-like function augments each plane wave.

The most effective technique to linearize Slater's APW method is to use the usual LAPW method with the extra restriction on the PWs of matching in value and slope to the solution inside the sphere. Using the conventional APW basis can greatly increase its efficiency; naturally, this requires $u_l(r, E_l)$ to be at constant energy E_l to maintain the linear eigenvalue issue. To have sufficient variational flexibility in the radial basis functions, one then adds a new local orbital (lo).

$$\Phi_{\mathbf{K}_n} = \begin{cases} \sum_{lm} [A_{lm,\mathbf{k}_n} u_l(r, E_l)] Y_{lm}(\hat{r}), & r \in S_t \\ \frac{1}{\sqrt{\omega}} e^{i\mathbf{k}_n \cdot \vec{r}}, & r \in I, \end{cases} \quad (2.26)$$

As a result, we build basis functions with "kinks" at the sphere border, necessitating the inclusion of surface components in the Hamiltonian's kinetic energy component. But take note that the entire wave function is, of course, differentiable and smooth. The LAPW (APW+lo) approach, in its general form, increases the charge densities in a comparable manner and the potential in the following way. Here, the equation contains the potential expansion coefficients in terms of spherical harmonics

$$V_{\mathbf{r}} = \begin{cases} \sum_{LM} V_{LM}(r) Y_{LM}(\hat{r}), & r \in S_i \\ \sum_{LM} V_{\mathbf{K}} e^{i\mathbf{K}\cdot\mathbf{r}}, & r \in I, \end{cases} \quad (2.27)$$

As a result, no shape approximations are made; this process is commonly referred to as the "full-potential" technique. In early band computations, the "muffin-tin" approach was meant to preserve just the $\mathbf{K} = 0$ component in the second expression of the equation and only the $l = 0$ component in the first. This (far older) method is equivalent to calculating the volume average in the interstitial zone and the spherical average inside the spheres.

2.4.3 Maximally Localized Wannier Function

Transformation of the extended Bloch orbitals alternatively in the form of localized Wannier functions [68, 69] are called Maximally Localized Wannier Functions to compute the band dispersion curve using the hybrid functional; this band structure gives us precise band edge value and effective mass over the Brillouin zone.

$$\langle \mathbf{R}n | \mathbf{r} | \mathbf{0}m \rangle = i \frac{V}{(2\pi)^3} \int d\mathbf{k} e^{i\mathbf{k}\cdot\mathbf{R}} \langle u_{n\mathbf{k}} | \nabla_{\mathbf{k}} | u_{m\mathbf{k}} \rangle \quad (2.28)$$

$$\langle \mathbf{R}n | r^2 | \mathbf{0}m \rangle = -\frac{V}{(2\pi)^3} \int d\mathbf{k} e^{i\mathbf{k}\cdot\mathbf{R}} \langle u_{n\mathbf{k}} | \nabla_{\mathbf{k}}^2 | u_{m\mathbf{k}} \rangle \quad (2.29)$$

Since these equations allow one to describe the localization functional Ω in terms of the matrix elements of $\nabla_{\mathbf{k}}$ and $\nabla_{\mathbf{k}}^2$, they lead us to the necessary connections with underlying Bloch formalism. In addition, they make it possible to determine the impact on localization of any unitary transformation of the $|u_{n\mathbf{k}}\rangle$ without having to do computationally expensive (particularly when using plane-wave basis sets) scalar product calculations again. Thus, on a regular mesh of \mathbf{k} points, we get the Bloch orbitals $|u_{m\mathbf{k}}\rangle$ and utilize finite differences to compute the aforementioned derivatives.

2.4.4 van der Waals Correction

The description of long-range dispersion forces is not effectively accommodated into the usual framework of any exchange-correlation functional which is required to accurately represent the interactions among the atoms in the 2D systems. Grimme developed the D2 and D3 corrections [70], a semi-empirical vdW correction technique that accurately includes the long-range dispersion forces into the conventional DFT, as a solution to this problem. The vdW correction is incorporated into the displacement energy components to rectify the total energy of the Kohn-Sham system solved using self-consistent field theory.

$$E_{disp} = -S_6 \sum_{i=1}^{N_{at}-1} \sum_{j=i+1}^{N_{at}} \frac{C_6^{ij}}{R_{ij}^6} f_{damp}(R_{ij}), \quad (2.30)$$

In the D2 scheme, a correction term (f_{damp} , at small distances) and a semi-empirical dispersion potential $C_6 R^{-6}$ are added to the Kohn-Sham energy. The dispersion correction factor E_{disp} , which is integrated into the Kohn-Sham energy for the D3 scheme, is formed by the sum of the two-body and three-body energies. However, we have solely taken into account the Grimme-D2 adjustment to maintain uniformity in the energy estimate for all systems examined in this study.

2.5 Optical property calculation

Optical absorbance computation is essential to understand the response of photocatalysts in the visible region of the electromagnetic spectrum. On one hand where it helps in the investigation of photogenerated charge carrier dynamics while on the other optical transition within the band gap can be calculated. A physical description of the interactions between light and matter is represented by a dielectric tensor. Principal refractive indices and optic axes are used to describe an anisotropic material. Neglecting the excitonic effects [71] and the local field corrections these optical properties are calculated based on the independent particle approximation. The momentum matrix elements that describe the

electronic transition between the conduction and valence bands in the crystal are used to calculate the imaginary part of the dielectric function given by [72]:

$$\epsilon_2^{IBZ}(\omega) = \frac{8\pi^2 e^2 \hbar}{m^2 \omega^2} \sum_{v,c} \int |M_{cv}(k)|^2 \delta\omega_{cv}(k) - \omega \frac{d^3k}{(2\pi)^3}; M_{cv}(k) = \langle u_{ck} | e \cdot \nabla | u_{vk} \rangle. \quad (2.31)$$

In this equation, the integration is initially calculated only in the first Brillouin zone. Symmetry operation is considered before the imaginary part is obtained.

While, the real part $\epsilon_1(\omega)$ is computed using the Kramer-Kronig relations from $\epsilon(\omega)$.

$$\epsilon_{1,\alpha,\beta}(\omega) = 1 + \frac{2}{\pi} P \int_0^\infty \frac{\omega' \epsilon_{2,\alpha,\beta}(\omega')}{\omega'^2 - \omega^2} d\omega' \quad (2.32)$$

Here, P denote the principal value of the integral. The linear optical response of the medium at all photon energies like absorption coefficient α , refractive index n , and the extinction coefficient k is described by the frequency-dependent complex dielectric function ($\epsilon(\omega) = \epsilon_1(\omega) + i\epsilon_2(\omega)$) whereas, for the study of optical absorbance of the system we calculate the absorption coefficient using:

$$\alpha(\omega) = \sqrt{2}\omega[\sqrt{\epsilon_1(\omega)^2 + \epsilon_2(\omega)^2} - \epsilon_1(\omega)] \quad (2.33)$$

Fig. 2.5 illustrates the variation of $\epsilon_2(\omega)$ and $\epsilon_1(\omega)$ with energy, the integrated region within the $\epsilon_2(\omega)$ curve demonstrates absorbance of the material, whereas $\epsilon_1(\omega)$ reflects the order of polarization hence the ability of material to store the incident energy.

2.6 Reaction Kinetics

2.6.1 Reaction Mechanics

Oxygen evolution reaction initiates with the adsorption of the water molecule over the suitable surface, the next step is the deprotonation reaction leading to

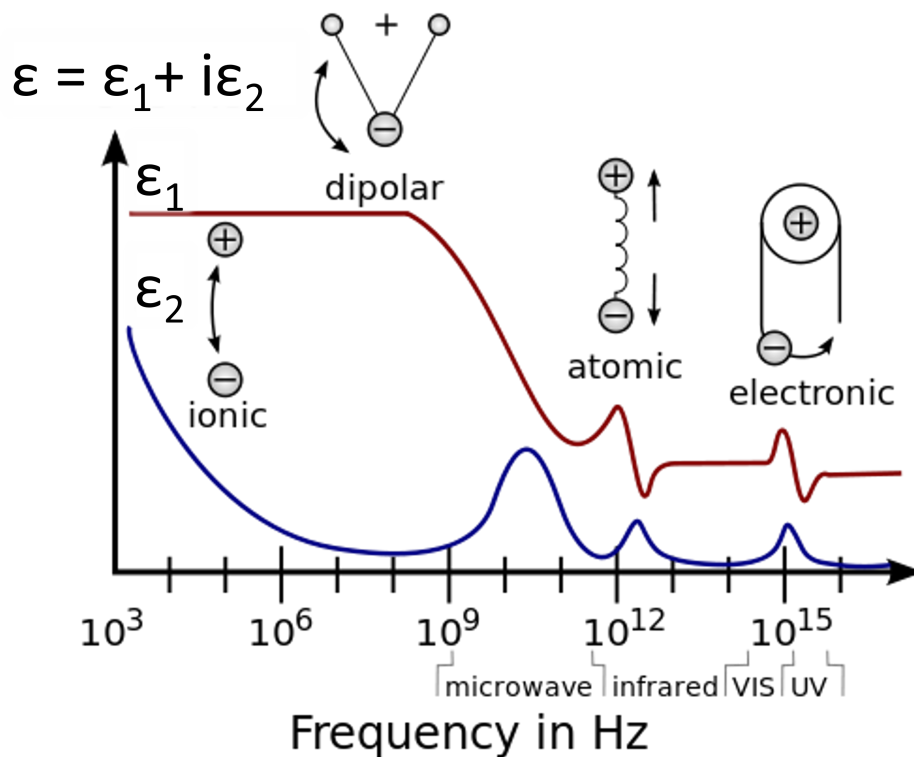
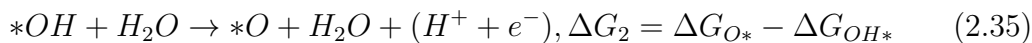
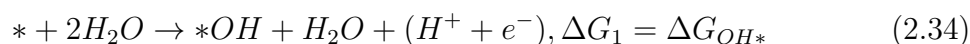


FIGURE 2.5: According to the Lorentz oscillator model, the real component ϵ_1 and the imaginary part ϵ_2 of the dielectric function path are shown in the picture as being dependent on the frequency ω [3].

the formation of hydroxyl (*OH). This *OH bonds chemically with the surface following further dissociation into *O and H^+ . The second water molecule on adsorption over the surface loses its proton and this dissociation of another H_2O into hydrogen and hydroxyl leads to *OH & *O association into *OOH. In the last step, this *OOH desorbs as the O_2 molecule after deprotonation, this process takes place according to Eqs. 2.34, 2.35, 2.36, 2.37. [73–75]



For the hydrogen evolution reaction, two methods are conventionally undertaken where

- single hydrogen atom is adsorbed over the most electronegative site of the

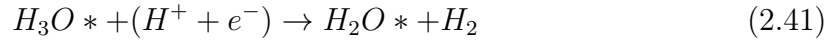
whole surface, this electronegative site is derived from the l owdin charge analysis.

- a whole hydronium (H_3O) molecule is adsorbed and adsorption energy is calculated where extra water molecules simulate the more realistic situation in an acidic medium

Thereafter $\Delta G_{H/H_3O}$ is calculated using the $\Delta E_{*H/*H_3O}$ following Eqs. 2.38, 2.39, 2.40, 2.41. The energy barrier is thus considered to be $|\Delta G_{*H/*H_3O}|$, which is defined as the extra energy required for the reaction to be completely feasible computed by Eq.2.49 [75]. Here * represents the surface of the catalyst.



The role of extra water molecules in the adsorption of H can be understood from the following two equations,



To calculate the adsorption energy (ΔE_{ads}) for all the reaction intermediates to calculate the free energy change following formalism is used:

$$\Delta E_{ads} = E_{adsorbent+adsorbate} - (E_{adsorbent} + E_{adsorbate}) \quad (2.42)$$

$$\Delta E_{ads}^{H_2O} = E_{H_2O-Substrate} - (E_{Substrate} + E_{H_2O}) \quad (2.43)$$

$$\Delta E_{ads}^{*OH} = E_{OH-Substrate} - (E_{Substrate} + E_{H_2O} - 1/2E_{H_2}) \quad (2.44)$$

$$\Delta E_{ads}^{*O} = E_{O-Substrate} - (E_{Substrate} + E_{H_2O} - E_{H_2}) \quad (2.45)$$

$$\Delta E_{ads}^{*OOH} = E_{OOH-Substrate} - (E_{Substrate} + 2 \times E_{H_2O} - 3/2 \times E_{H_2}) \quad (2.46)$$

$$\Delta E_{ads}^{*H} = E_{*H-Substrate} - (E_{Substrate} + 1/2E_{H_2}) \quad (2.47)$$

$$\Delta E_{ads}^{*H_3O} = E_{*H_3O-Substrate} - (E_{Substrate} + E_{H_2O} + E_{H_2}) \quad (2.48)$$

The standard Gibbs free energy change, ΔG , represents a physical or chemical process' thermodynamic favorability. The process is thermodynamically favorable

when $\Delta G < 0$. The following formula may be used to get the value of ΔG for a given process directly from the values of ΔH and ΔS :

$$\Delta G = \Delta E + \Delta ZPE - T\Delta S + \Delta G_{pH} + \Delta G_U \quad (2.49)$$

Here, ΔE is the overall energy change estimated from DFT studies, ΔZPE is the change in zero-point energies, ΔS is the entropy change, and T is the temperature. $\Delta G_U = -eU$ (U is the potential measured against NHE), $\Delta G_{pH} = -k_B T \ln(10) \times pH$, ΔG has been computed at $pH = 0$. Nørskov's [73, 74] approach is used to calculate the free energy change in the oxidation/reduction reaction. For OER and HER, the step with maximum free energy difference is the reaction barrier ($\Delta G^{HER/OER}$), and its corresponding overpotential ($\eta^{HER/OER}$) is defined as,

$$\eta^{HER/OER} = \text{Max}[\Delta G_i] - 0.0/1.23V, \quad (2.50)$$

here i denote the intermediate steps.

2.6.2 Reaction Barrier Calculation

Climbing image Nudged Elastic Band (CI-NEB) can be used to compute the transition state (TS) configuration at the saddle point in addition to the minimum energy path (MEP) for the reaction as shown in Fig. 2.6. One variation to the ascending image NEB approach pushes the image with the most energy up to the saddle position. The spring forces along the band are not visible in this view. Rather, the real force along the tangent is reversed in this image. The image attempts to decrease its energy in all directions and enhance it along the band in this manner. This image will converge at the precise saddle position [4, 5]. It is feasible to identify the precise barrier and locate the climbing image at the saddle point using the CI-NEB approach. We should examine the chemical reaction and determine the relevant transition state using the CI-NEB approach since it performs better in transition state searches than the standard NEB method. In terms of quality, the ascending image travels along the elastic band up the potential energy surface and down the potential surface perpendicular to the band. The remaining images in the band are meant to define the one degree of freedom where energy maximization is implemented. The images in the band provide a decent estimate

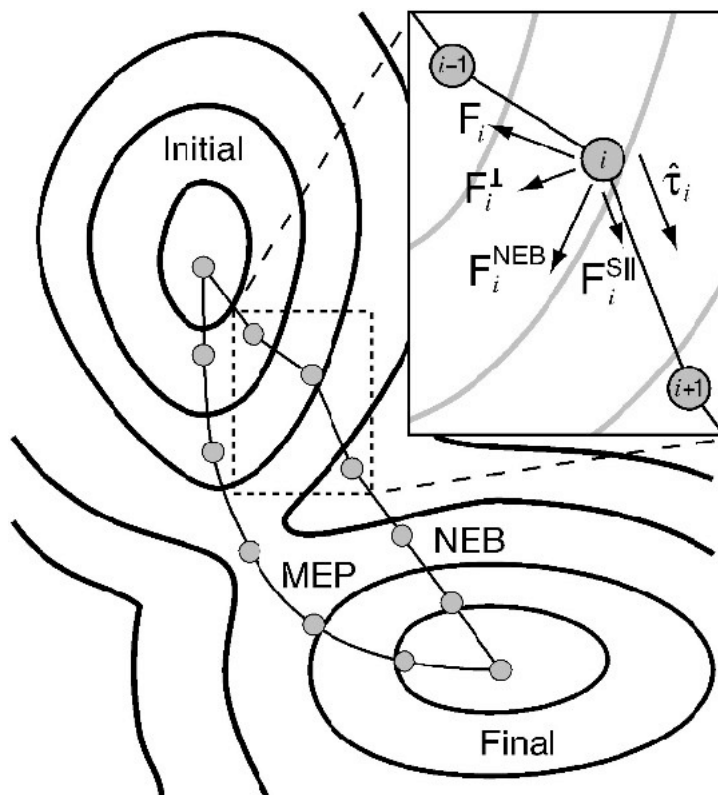


FIGURE 2.6: Climbing Image Nudge Elastic Band plot showing the minimum energy path, along with the tangential forces to compute the reaction barrier [4, 5]

of the reaction coordinates near the saddle point since they ultimately converge to the MEP. The ascending image will converge to the saddle location if the CI-NEB approach converges. Making one of the images a climbing image doesn't incur any additional costs because all of the images are being relaxed at the same time.

2.6.3 Parabolic Approximation based Effective Mass Calculation

The band gap value of the layered system is calculated from the ground state electronic property. The whole photocatalytic activity cannot be determined by the mere presence of a band gap in the visible spectrum; thus, the charge carrier mobility and their recombination rate play a crucial part in analyzing the charge dynamics in the system. Reduced effective mass ($m^* = e\tau/\mu$, where m^* is effective mass, e is the electronic charge, τ is collision time, and μ is carrier

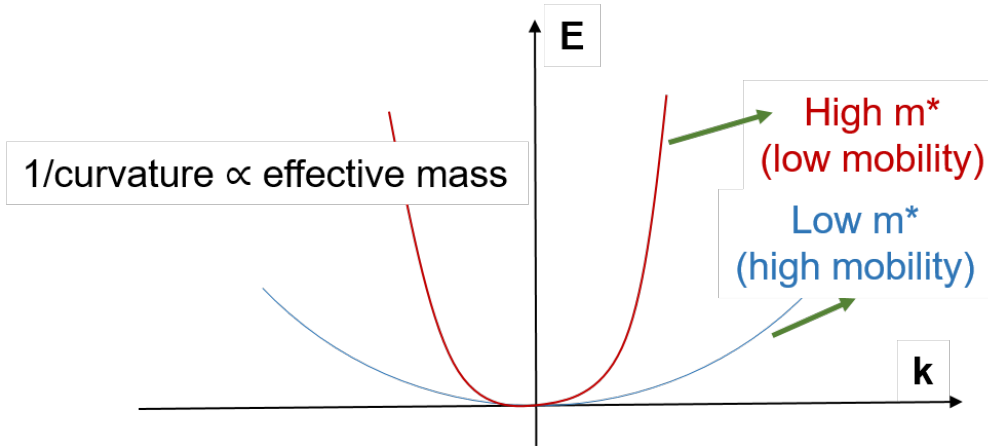


FIGURE 2.7: E-k diagram representing bands of different curvature, and the parabolic fitting specifying the curvature depending on mobility.

mobility) results in higher charge carrier mobility, which not only shortens the duration of photo-induced $e^- - h^+$ pair transport within the material but also accelerates charge displacement over the surface to prevent charge accumulation and provide a clean surface for redox activity enhancement. The effective masses of electrons and holes (m_e^* and m_h^*) have been determined using the parabolic band approximation, where E is the energy of the conduction band minima for electrons and the valence band maxima for holes. Effective mass and its ratio ($\beta = m_e^*/m_h^*$) are computed from the band structure. Additionally, for $e^- - h^+$ pairs, β correlates to the variation in the effective mass; smaller variance values indicate quick recombination with slow activity, and vice versa.

$$E = \frac{\hbar^2 k^2}{2m} \quad (2.51)$$

$$\text{Effective mass}(m^*) = \hbar^2 \left[\frac{\partial^2 E}{\partial k^2} \right]^{-1} \quad (2.52)$$

With parabolic bands as shown in Fig. 2.7, the electron will travel with m^* , which is correlated with the band's curvature, much like a free particle. The local slope and curvature of the E-k equation must be employed to determine the mobility of the particle with energy E in non-parabolic bands since m^* is not consistent over an entire band for different k-regions. Parabolas can be used to approximate the

form of the top of the VB and the bottom of the CB, resulting in effective masses of holes and electrons, respectively.

2.7 Computational Codes

We employ the open-source Quantum Espresso software[76], which is an integrated suite for performing bulk and nanoscale electronic structure computations and materials modeling. DFT, plane wave approximation, and pseudopotential techniques serve as their foundations. With this package, we calculated the ground state eigenenergies of the bulk and low dimensional periodic systems using first-principles calculations under self-consistent field formalism. We use non-self-consistent field formalisms to do computations for electronic structure calculations, where we calculate the electronic eigenstates as a function of crystal momentum. We can compute electronic charge densities, execute calculations using vdW dispersion corrections, compute electronic structure, and compute the density of states and partial/orbital density of states after we perform structural relaxations and optimizations with this code because of its extreme versatility. The open-source nature of the Quantum Espresso code allows it to be interfaced with various computational codes to calculate additional material characteristics, which is another benefit. Several individuals in a dynamic computational physics group create scripts that are readily interfaced with Quantum Espresso, so augmenting its functionality. Optical characteristics of the dielectric tensor have been computed using the *epsilon.x* [76] package, which is integrated into the Quantum Espresso code. Using WannierTools [69] code, we computed and examined band structure for hybrid functional implementation by utilizing the maximum localized functions. For crystal structure generation and visualization, we have used VESTA, BURAI, and XCrysden software. We have also considered Wien2K code[59] which is based on the FP-LAPW approach in a few cases.

